1.4 µm Pixel, 8 MP, > 5 µm epi, RGB-IR Image Sensor

Orit Skorka, Stan Micinski, Andrew Perkins, Bob Gravelle, Xunzhi Li, and Radu Ispasoiu
ON Semiconductor, Intelligent Sensing Group, USA, email: Radu.Ispasoiu@onsemi.com

***Abstract*—**Image sensors with 1.4 µm pixel size, 8 MP array, stacked BSI, 65 nm technology, have been fabricated with thick (>5 µm) epi silicon as a basic pre-requisite condition for increased near-infrared (NIR) response. Two backside surface processing variants were prepared and patterned with RGB-IR color filter array: one with NIR-enhancement inverted pyramids, and a baseline without NIR-enhancement features. An analysis is provided on the performance of these structural variants for RGB-IR imaging. Application specific recommendations are made for the pixel variants developed.

I. Introduction

Stacked BSI CMOS image sensor with 1.4 µm pixel size and 8 MP array was developed in 65 nm technology with silicon epi thicker than 5µm, backside deep trench isolation (BDTI), and two backside surface processing variants: Pixel "A" with light trapping inverted pyramidal structures [1]; Pixel "B" baseline without backside surface processing features.

Both types of structures were patterned with 4x4 kernel RGB-IR color filter array (CFA). Figure 1 presents schematic cross-sections and CFA pattern. RGB-IR color filter array has become an advantageous solution for applications including surveillance and automotive imaging. However, to the best of our awareness, insufficient literature has so far been dedicated to the RGB-IR imaging analysis and optimization of image sensor near-infrared (NIR) response for RGB-IR image quality. In this work, we are aiming at demonstrating RGB-IR imaging performance criteria with a new 8 MP sensor developed for a broad range of applications requiring the best trade-offs between high color accuracy, high NIR response, high resolution, high dynamic range, good low light performance, low power consumption and low cost.

II. Optical Modeling and Characterization

Pixel quantum efficiency (QE) in NIR can be increased by backside surface processing techniques that increase the optical path of NIR photons. However this technique increases optical cross-talk and, therefore, degrades pixel point spread function (PSF). BDTI helps reduce crosstalk, especially when trench depth becomes comparable with the silicon epi thickness, but this also introduces fabrication challenges and cost increase. Finite difference time domain (FDTD) modelling was applied to understanding trade-offs for optimizing pixel optical path design for cost-effective fabrication. Pixel PSF can be measured by carefully aligned single pixel illumination techniques, but the procedure requires high precision test equipment or complex analysis [2]. Modulation transfer function (MTF) is often characterized through the line-spread function using the well-established slanted-edge method [3]. To demonstrate the correlation between single-pixel illumination PSF and slanted-edge MTF, the two illumination configurations were implemented into an FDTD modeling of light propagation in Pixel A, as shown in Figure 2. For the PSF method the MTF is calculated from the simulated response curve of Gaussian source sweeps through the pixel pitch (over -sampling). For the edge-response method first the edge spread function (ESF) is determined from sweeps of the edge (light block) through the pixel pitch and then the derivative of the ESF is used to generate the line spread function (LSF) from which the MTF is calculated. In each case the response is based on calculated QE at 550 nm from the optical absorption within the photo diode of each pixel. Figure 3 presents MTF curves of Pixel A as obtained with the two illumination scenarios. It is evident that the FDTD MTF simulations with single-pixel and edge illumination produce similar results.

Having established the correlation between PSF simulation and the experimentally-calibrated edge response simulation, the PSF FDTD technique was further utilized, with the benefit of visually intuitive energy propagation models. PSF was simulated for the nominal BDTI depth for Pixel A and B as well as for a hypothetical full depth BDTI variant of Pixel A. Figure 4 presents the wave propagation energy diagrams for the three simulated structures at 940 nm. It is evident from Figure 2 (a) and Figure 4 (a) that optical cross-talk increases with wavelength. It is also evident from Figure 4 (a) and (b) that optical cross-talk is more dominant in Pixel A than in Pixel B. Figure 5 presents measured MTF results of Pixel A and Pixel B and simulated MTF of the full-depth BDTI variant of Pixel A. Measurement results confirm that the inverted pyramid scatter enhancement for increasing NIR wave optical path is detrimental to optical cross-talk. Simulation results show that mitigation can be achieved via the deepest BDTI that available fabrication process recipes can achieve.

III. Image Quality

Image quality of the two RGB-IR pixel variants was evaluated according to the following metrics: spatial resolution, spectral purity of visible channels under any amount of infrared (IR) radiation in the scene illuminant, and dynamic range drop of visible channels due to IR radiation.

Figure 6 (a) presents normalized quantum efficiency (QE) curves of Pixel A and B. It shows that, at 940 nm, QE of Pixel A is 1.8 times higher than QE of Pixel B. To minimize camera size and weight, a dual band-pass filters (DBPF), which includes a band-pass filter that covers most of the visible band and a narrow pass filter in the NIR, can be used with RGB-IR sensors to achieve color and NIR images interchangeably. Figure 6 (b) presents normalized transmission curve of a commercially available industry standard visible-940 nm DBPF. It also shows normalized spectral power distribution (SPD) of solar irradiance [4]. Figure 6 (c) presents the photo-

generation rate, G_{ph}, curves of Pixel A and B with the same DBPF with sunlight illumination.

In RGB-IR imaging applications, when, in most common natural illumination conditions, all pixels are exposed to a spectral combination of visible and NIR radiation, a special processing block should be added to the color pipeline to subtract the NIR signal in order to prevent color artifacts due to NIR-generated signal. Although NIR signal can be subtracted from the total photo-generated signal before color processing, it still occupies some of the pixel well capacity and, therefore, lowers the dynamic range for color imaging. Figure 7 presents a set of Macbeth color-checker chart images that were captured with camera modules with Pixel A and B sensors in a light booth with a 5,500K CCT and 940 nm LED illuminants. Image #1 of both sensors was captured with the 5,500K CCT LED illuminant only, which does not have any illumination components in NIR. Figure 7 (a) and (b) presents the color processed images, which are considered as reference color images. Both images look very similar. Image #2 was captured when the intensity of the 5,500K CCT LED illuminant remained unchanged, and the 940 nm LED was turned on. Figure 7 (c) and (d) show color images as obtained after processing through a pipeline that included an IR subtraction block [5]. Colors appear more saturated and with higher blue content in the Pixel A image. The yellow patch becomes white due to green and red pixel saturation. Figure 7 (e) and (f) present the NIR image of Image #2, where it is evident that Pixel A has higher NIR responsivity.

To complement the controlled illumination analysis with a practical RGB-IR imaging situation, we captured outdoor images during daytime with camera modules with both Pixel A and B sensors and the same DBPF with transmittance spectrum shown in Figure 6(b). These images were processed with the same pipeline but coefficients that matched sunlight SPD. Figure 8 presents color and NIR images that were obtained from the raw RGB-IR images. Color patches in the color chart appear more saturated in the color image of Pixel A, but differences are small. The foliage area behind the chart is clearly brighter in the NIR image of Pixel A. In both color and NIR images, the edge details, such as license plate characters shown in inserts, are sharper with Pixel B -which is in agreement with MTF results and FDTD modeling. Although the section of the NIR image of Pixel A is brighter due to the higher NIR responsivity of Pixel A, the fine object details are buried in noise and cannot be detected with high confidence. Detection metrics that combine signal-to-noise ratio (SNR) and MTF, like noise equivalent quanta (NEQ) and Ideal Observer SNR (SNRI) [6], can be useful as figures of merit when there is a trade-off between SNR and MTF.

In summary, the NIR-enhanced Pixel A is advantageous for RGB-IR surveillance imaging where stronger NIR responsivity is the key factor. Pixel B without the NIR enhancement pyramids has sufficient NIR response from the thicker silicon epi and has the benefit of better MTF with a cost effective mature fabrication process with partial BDTI.

IV. Conclusion

This work discussed trade-offs in fabrication and image quality metrics of RGB-IR image sensors using two variants of a 1.4 µm pixel image sensor with silicon epi that is greater than 5µm. FDTD light path simulations and measured MTF showed that backside surface processing features for NIR enhancement increase crosstalk and lower spatial resolution and that this can be mitigated by deeper BDTI structures, which increase complexity and cost of fabrication process. Analysis of images that were captured both in controlled illumination environment and outdoors demonstrated correlation with MTF predictions as well as an additional trade-off between dynamic range of color images and NIR responsivity. Among the two variants, the NIR-enhanced one is preferred for applications where high NIR responsivity is crucial while the other variant is the preferred choice for applications that would benefit from higher MTF.

Acknowledgment

The authors gratefully acknowledge the contributions of Rujul Desai, Richard Zhang, and Danyu Li to the work.

References

[1] P. Campbell and M. A. Green, "Light trapping properties of pyramidally textured surfaces," *Journal of Applied Physics,* pp. 243-249, 1987.

[2] V. Lenchenkov, O. Skorka, R. Gravelle, U. Boettiger and R. Ispasoiu, "Characterization of Image Sensor Resolution by Single-Pixel Illumination," in *Electronic Imaging*, San Francisco, 2018.

[3] *ISO 12233:2017 Photography -- Electronic still picture imaging -- Resolution and spatial frequency responses,* 2017.

[4] ASTM G173, "Standard Tables for Reference Solar Spectral Irradiances: Direct Normal and Hemispherical on 37° Tilted Surface," 2020.

[5] ON Semiconductor, *AND9492/D RGB-IR Sensors and Image,* 2016.

[6] P. Kane, "Signal detection theory and automotive imaging," in *Electronic Imaging*, 2019.

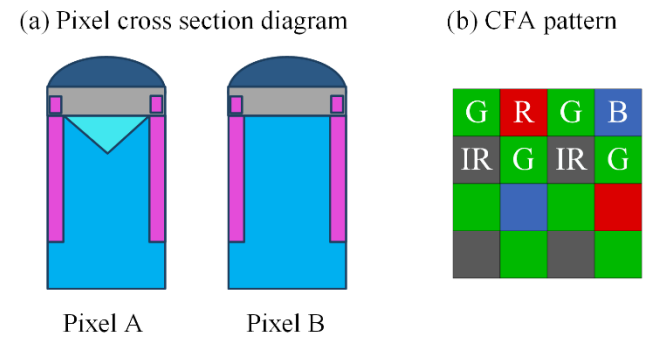

Figure 1. (a) Cross-section diagram of Pixel A and B. (b) CFA 4x4 unit cell pattern.

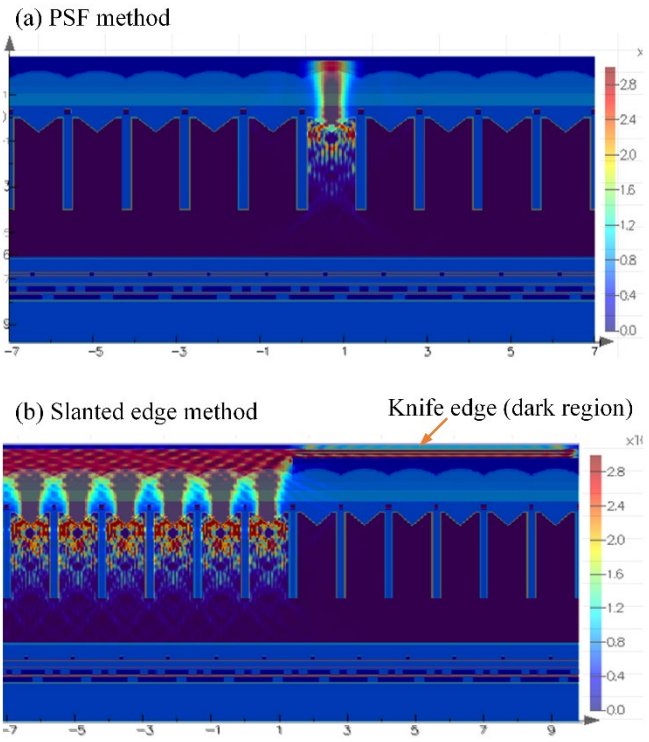

Figure 3. FDTD simulations of Pixel A structure to obtain MTF at 550 nm using (a) the PSF method and (b) the slanted edge method.

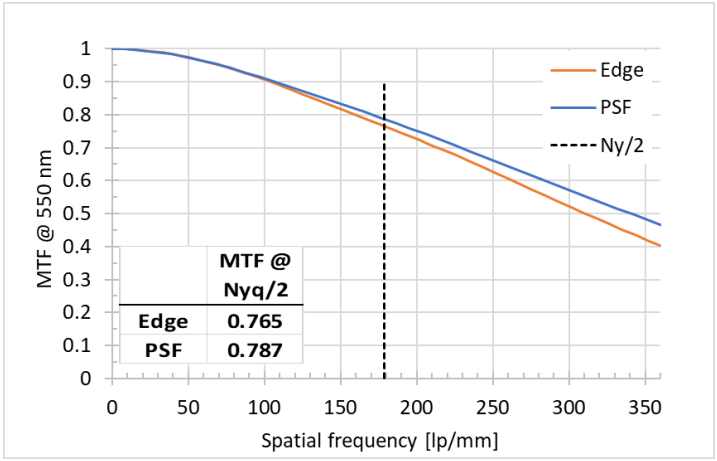

Figure 5. Simulated MTF curves of Pixel A at 550 nm using the PSF and the edge methods.

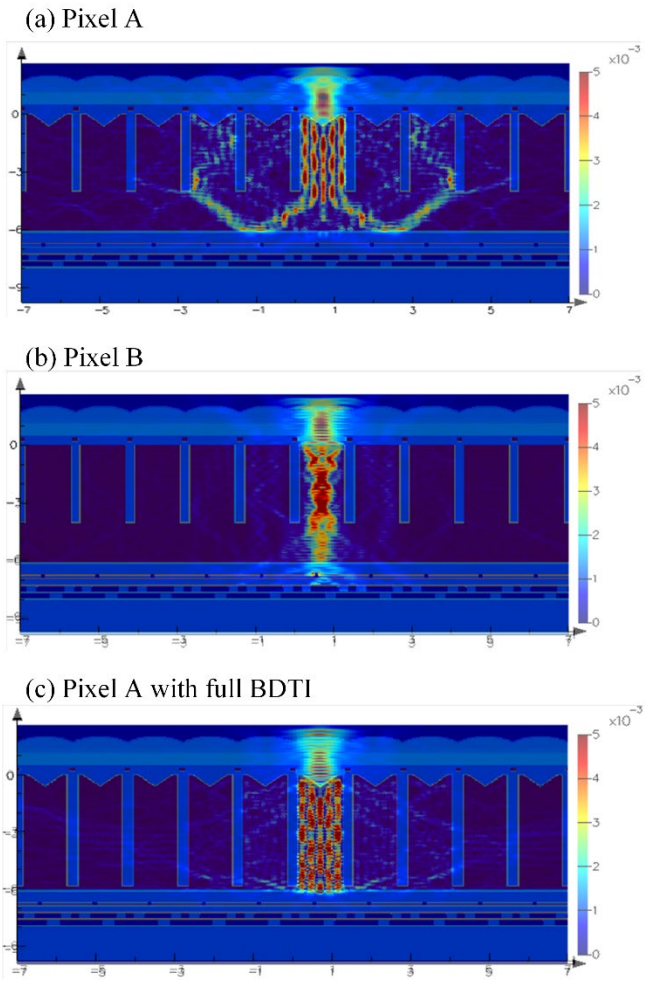

Figure 2. FDTD modelling of 940 nm radiation propagation in: (a) Pixel A, (b) Pixel B; (c) Pixel A with full depth BDTI.

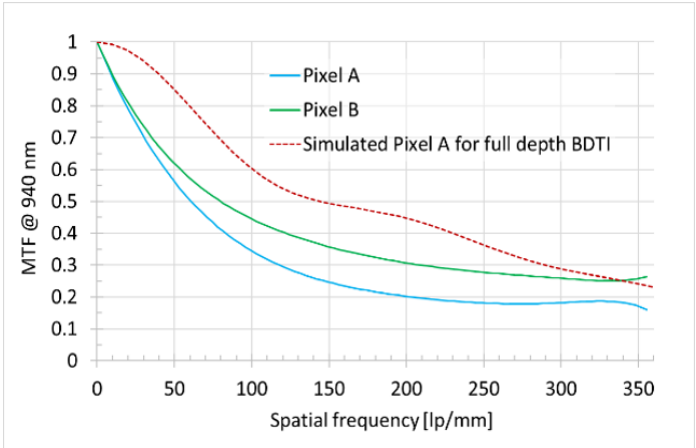

Figure 4. MTF curves of the structures from Figure 4 at 940 nm.

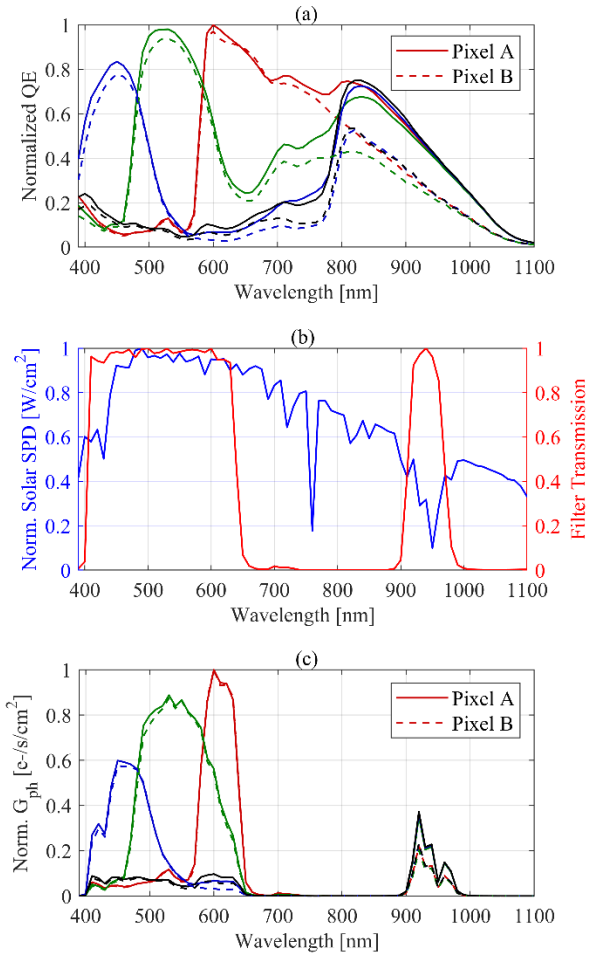

Figure 6. (a) QE sets of Pixel A and B, (b) Solar spectral irradiance and transmission curve of a visible-940 nm DBPF, and (c) Pixel A and B photo generation rate with the illuminant and filter from (b).

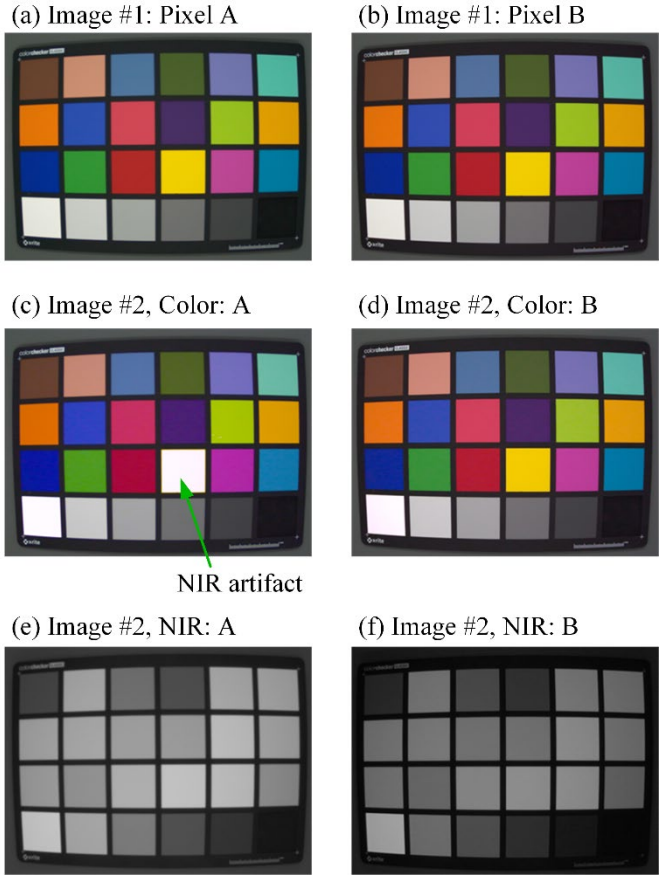

Figure 7. Pixel A and B Macbeth chart captures: (a) and (b) Color image of Image #1; visible light only; (c) and (d) color images of Image #2; (e) and (f) NIR images of Image #2. The illuminant included visible and NIR light components.

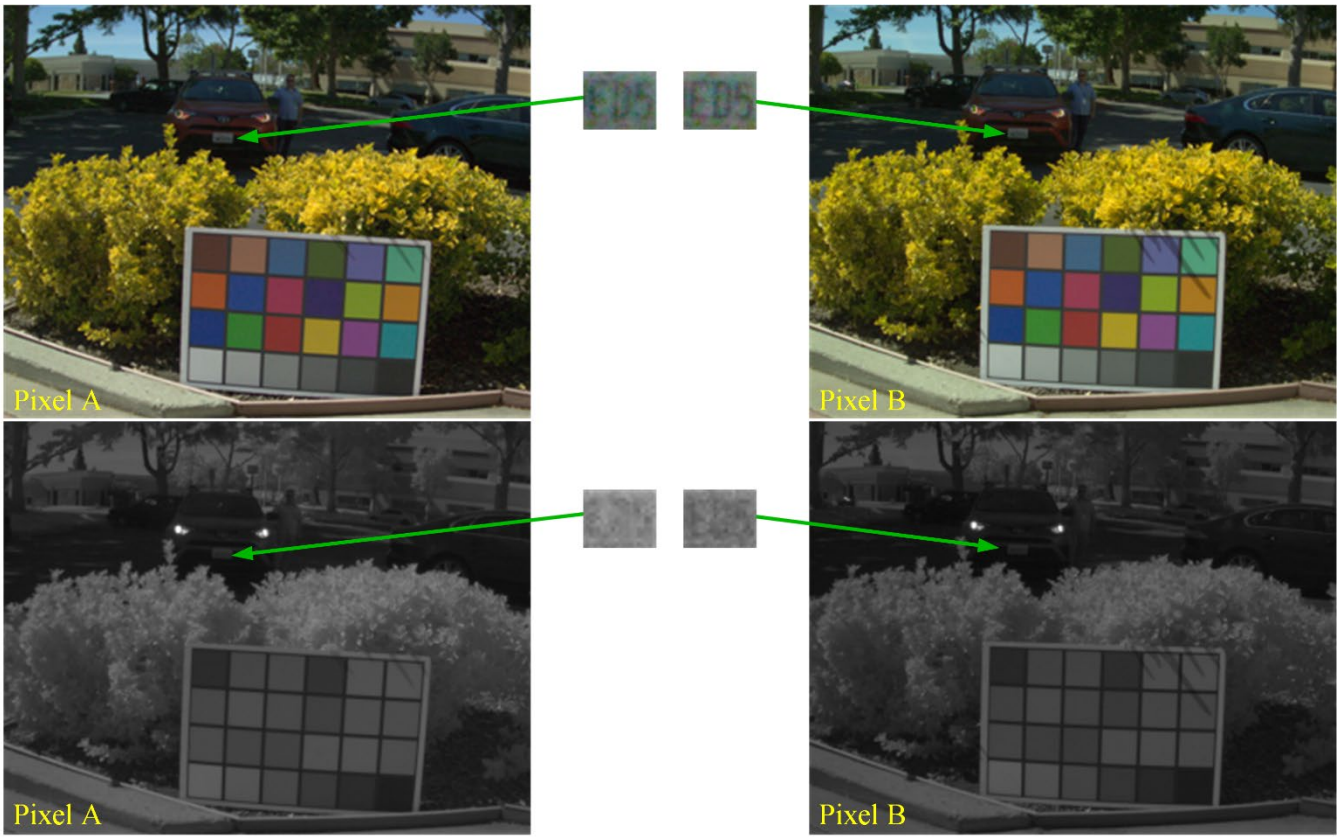

Figure 8. Color and NIR images of RGB-IR captures with Pixel A and B. The NIR image of Pixel A is brighter, but license plate characters are sharper with Pixel B.